



Research Article

Effects of intake manifold geometry in H₂ & CNG fueled engine combustion

Rafaa SAAIDIA¹, Ons GHRIS², Hasan KOTEN^{3*}, Mohammed M ALQURAI⁴,
Abdallah BOUABIDI^{1,5}, Mamdouh EL HAJ ASSAD⁶

¹Mechanical Modeling, Energy and Material (M2EM), National School of Engineering of Gabes (ENIG), University of Gabes, Gabes, 6029, Tunisia

²National Engineering School of Gabes (ENIG), Research Laboratory “Processes, Energetics Environment and Electrical Systems”, Gabes University, Omar Ibn Kattab ZRIG, Gabes, 6029, Tunisia

³Department of Mechanical Engineering, Istanbul Medeniyet University, Istanbul, 34700, Türkiye

⁴Department of Mechanical Engineering, College of Engineering, University of Bisha, Bisha, P.O. Box 001, 61922 Kingdom of Saudi Arabia

⁵Higher Institute of Industrial Systems of Gabes (ISSIG), Slaheddine El Ayoubi Street, Gabes, 6011, Tunisia

⁶Department of Sustainable and Renewable Energy Engineering, University of Sharjah, Sharjah, 27272, United Arab Emirates

ARTICLE INFO

Article history

Received: 13 April 2023

Accepted: 15 August 2023

Keywords:

Gas Engine; Intake Manifold;
Acoustic; Natural Supercharging

ABSTRACT

This study attempted to identify the effect of optimized intake manifold geometry on the behaviors and emission level of hydrogen compressed natural gas (H₂CNG) fueled engine. For this purpose, a commercial Hyundai Sonata spark ignition engine (SIE) is modified to operate with CNG and hydrogen blend. The optimal intake pipe length was predicted using an analytical acoustic method. A new intake manifold is designed and implemented utilizing natural supercharging managed by over-pressure waves acoustic propagation. Several tests are conducted on the engine using the new manifold with a speed range from 1000 to 5000 rpm. Based on various engine speeds, the variation of brake torque (BT), in-cylinder pressure, NO_x and CO emissions investigated by using gasoline, CNG and hydrogen CNG blend (HCNG) fueled engines via external mixtures. The first finding of the study is that the novel geometry improves the in-cylinder pressure by 10% at 3500 rpm. However, high engine speeds show a reduction of 14% in NO_x and 40% in HC while speeds below 2000 rpm reduce CO by 40%. The second finding is that the new optimized geometry serves to get rid of both the auto-ignition and the backfire for high ratio of hydrogen in the blend.

Cite this article as: Saaidia R, Ghriss O, Koten H, Alquraish MM, Bouabidi A, El Haj Assad M. Effects of intake manifold geometry in H₂ & CNG fueled engine combustion. J Ther Eng 2024;10(1):153–163.

*Corresponding author.

*E-mail address: hasan.koten@medeniyet.edu.tr

This paper was recommended for publication in revised form by
Regional Editor Ahmet Selim Dalkilic



INTRODUCTION

Reducing pollution and enhancing performance of Internal Combustion Engine (ICE) is one of the main goals of research worldwide. In this context, several works have been conducted to optimize geometrical and operating parameters. For example, Heywood [1] observed that independently of the internal combustion engine (ICE) operating system, its fuel type and its strokes number, its performance and emissions characteristics were directly conditioned by the air mass introduced into its cylinders. Indeed, this air mass determines the maximum fuel load that could be introduced into the cylinders, and the amount of energy that the engine is capable of supplying. However, as was demonstrated by Sharma et al. [2], not all the energy was transformed into mechanical energy on a shaft. Part of this energy was converted into unburnt exhaust losses and heat losses. Hence, the intake manifold was considered by Priyadarsini [3] and Chaubey et al. [4] as a fundamental component for an optimal ICE operation.

Moreover, the choice of an optimal geometry of the intake manifold was considered essential to improve the engine performance. Heywood [1] proposed the insertion of the intake manifold between the throttle air-fuel blend or air pure and the cylinder head on the side of the intake ports. They showed that the insertion of the intake manifold enhanced the ICE performance. Recently, a new upsurge of interest has been accorded with the improvement of intake. Chaubey and Tiwari [4] carried out a series of Computational Fluid Dynamics (CFD) to predict the flow distribution behavior inside each cylinder. They examined three manifold geometries. The first one is the standard manifold; the second configuration is equipped with branched helical runners and the third configuration is without curve of runner part. The research work has shown that the geometry of the intake manifold plays a crucial role in determining the in-cylinder flow characteristics of an internal combustion engine. The intake manifold is responsible for delivering the air-fuel mixture to the combustion chambers, and its design can significantly impact engine performance. Also, they showed that the point of the peak power was dependent on the runner diameter, whereas the power for high and low RPM was dependent on the intake runner length. Battista et al. [5] examined the ICE performance for the case of low temperature charge air. The researchers used an evaporator for producing cooled air. The study revealed that the air cooling reduced the fuel consumption and the CO₂ emissions. Silva et al. [6] conducted numerous numerical simulations to investigate the effect of the geometry of an intake manifold on the ICE performance. They investigated the volumetric efficiency for different lengths of the intake manifold runners. The work proposed a new variable configuration of the intake manifold. Their results showed that the proposed configuration enhanced volumetric efficiency and reduced fuel consumption as a function of rotation speed. Giannakopoulos et al.

[7] developed CFD simulations to simulate the fluid flow in the intake pipe. They performed simulations for two types of velocity profiles imposed in the inlet which are the parabolic and the power-law profiles. The results showed that the parabolic velocity profile enhanced the turbulence. Benajes et al. [8] proposed a new model using the acoustic-wave theory to examine the geometrical parameters of the intake manifold. They found an optimum configuration of the intake manifold. Chalet et al. [9, 10] established numerical model to analyze the pressure waves in the manifold of ICE. They developed an experimental study to measure the pressure signal evolution and the new model was validated with their experimental data.

Costa et al. [11] conducted numerous experiments to analyze the geometrical parameters effect on the performance of spark ignition engine. They investigated the effect of intake pipe length and diameter. It was revealed that the effect of two dimensions was dependent on the engine speed. The study demonstrated that the intake pipe with longer length and smaller diameter had the best performance at low speed, whereas the intake pipe with shorter length and larger diameter had the best performance at high speed.

Sadek et al. [12, 13] examined the ICE performance with a new intake configuration. In this study the researchers proposed a new spiral-helical with different configuration. It was revealed that the new proposed design enhanced the engine performance and significantly reduced the emissions.

Och et al. [14] proposed a mathematical model for optimizing the volumetric efficiency of a single cylinder diesel engine. The work carried out essentially aims to monitor the evaluation of volumetric efficiency for different lengths of inlet duct. The results reveal that the length of the intake duct has a greater effect on the volumetric efficiency than that of the exhaust. Machado et al. [15] proposed a new intake system equipped with variable duct length. They revealed that the new design enhanced the engine performance. Gocmen et al. [16] carried out series of CFD simulations to test different configurations of the intake manifold. They examined a standard intake manifold and two modified configurations. The work used the standard k-epsilon turbulence model to simulate the turbulent flow inside the intake. The velocity and pressure distributions were presented for all the proposed geometries. The results found that the new manifold had a significant effect on the pressure distribution and reduced the exhaust emissions.

These efforts resulted in optimizing the amount of air introduced into the cylinder. Within this context, Soto et al. [17] revealed that the supercharging was obtained due to the acoustic wave propagation phenomenon in the intake pipe. This was explained by Hiereth et al. [18] and Hadjkacem et al. [19], who confirmed that the supercharging occurred without any modification or addition to the system because it was an acoustic or natural supercharging.

A further development in research related to this topic was the modeling of the intake line behavior. This approach adopted two techniques. The first one, called the pulsed quarter-wave resonance, was implemented by Borel [20] and Desmond and Richard [21]. The second technique, called the Helmholtz resonator, was implemented by Samuel et al. [23] and Bortoluzzi et al. [24]. Borel [20] theorized that the quarter-wave resonance method of cylinder natural supercharging was directly related to the phenomenon of pressure wave propagation moving at the acoustic speed. This scholar explained that the existence of this phenomenon was linked to the unstable operation conditions of engines. Indeed, the periodic opening, closing of the intake and exhaust valves and the pistons movement were considered the sources of the unsteady flows that gave rise to the pressure waves. That was how they promoted the cylinder filling at the intake valves level by pushing a maximum air-fuel fresh charge into the combustion chamber. Within the quarter-wave resonance technique, Margary et al. [25] conducted experimental studies at started and rated engine speeds. Their experiments proved that the acoustic phenomena significantly influenced the volumetric efficiency in the intake manifold. More accurately, they revealed that an improvement of 9% was obtained in volumetric efficiency when the intake pipes length adopted the quarter-wave method. Applying the resonator technique, Maftouni, et al. [26] investigated the intake manifold runner length effect on the volumetric engine efficiency. Their analysis was performed using CFD simulation for different engine operating conditions. They observed that the volumetric engine efficiency was improved considerably when using the manifold geometry with 20% extended runners. Fontana et al. [27] conducted numerical and experimental studies to investigate different intake manifold geometries to improve its efficiency. The results showed that engine volumetric efficiency increased by 6% at 3500 rpm, consequently increasing the yielded power by 3.68 kW (4.93 hp).

Despite the abundance of research on this topic, shortcomings do still exist; namely, the focus on optimal geometry without considering the fuel mixture composition in the intake pipes. In addition, there is a failure to consider the engines using unconventional fuels before the total engine conversion. For this reason, this study attempts to use the

analytical acoustic method to predict the optimal intake pipes lengths. To achieve this goal, two novel devices are introduced. Firstly, a new collector using the natural supercharging generated by the over-pressure waves acoustic propagation is designed. Secondly, an optimized and cooled manifold is designed for the engine operating on a mixture of air / H₂-CNG carburetion (mixing process). The effect of hydrogen enrichment with CNG on the engine filling is investigated. Finally, emissions of the engine with the new geometry are measured and compared to those of an engine with a conventional geometry. The findings of this study are expected to have a positive impact on fuel consumption and the environment.

Engine Studied Geometry

This study took a Hyundai Sonata engine as a model. Table 1 exhibits the main characteristics of this engine. Due to the gas properties, as shown in Tables 2 and 3, the studied engine was modified and converted into Compressed Natural Gas (CNG) and adapted to the Hydrogen-Compressed Natural Gas (HCNG) operation. To perform a series of experiments, we designed and installed a test bench that allowed us to determine the experimental engine behavior with different intake manifold designs.

Figure 1 shows a photo of the apparatus used in the experimental system consisting of an internal combustion engine, a hydraulic brake, an acquisition card, an exhaust gas analyzer, a gas/petrol switch, an emulator, a lambda analyzer, and a computer.

Table 1. Engine characteristics

Engine Parameters	Value
Engine type	Hyundai Sonata
Displacement	1998 cm ³
Compression ratio	10.4:1
Cylinders	L4
Power	106 kW @ 6000 rpm
Fuel Supply System	Electronic Injection
Fuel	Gasoline

Table 2. Fuels properties

Characteristics	Gasoline	CNG	Hydrogen
Chemical formula	CH ₄ to CH ₁₂	Mixture of mainly 40% C ₃ H ₈ and 60% C ₄ H ₁₀	H ₂
Molecular weight	100–105	50	2.016 g/mol
Lower heating value (MJ/kg)	44.45	47.14	120.21
Fire point (°C)	230–500	~500	490
Ignition limits (% of volume)	1.0–7.6	1.5–9.5	4–75
Octane number	80–95	95–111.5	130



1- Engine; 2- Hydraulic brake; 3-Vaporiser; 4- Switcher; 5- Mixer; 6- Gas analyzer; 7-CassyLab card; 8- computer

Figure 1. Test bench components.

Gas Modeling in Intake Pipes

The macroscopic variables which characterize the thermodynamic equilibrium state of a fluid which is considered as an ideal gas are related by the equation of state $pV = nRT$, where p is the pressure, V is the volume, n is the number of moles and T is the temperature of the fluid.

Two types of compressibility coefficients were defined; namely, isothermal, and isentropic, which are expressed by Equation 1 as, respectively:

$$K_T = -\frac{1}{V} \left(\frac{\partial V}{\partial p} \right)_T \text{ and } K_S = -\frac{1}{V} \left(\frac{\partial V}{\partial p} \right)_S. \quad (1)$$

Longitudinal waves in intake pipe

Figure 2 shows the intake pipe model, where $\psi(x, t)$ represents the displacement at time t of the particles of section AB with respect to their rest position A_0B_0 of abscissa x and $\psi(x + dx, t)$ at the same time t . The displacement of the particles of the section CD is relative to its rest position C_0D_0 of abscissa $x + dx$.

The thickness of the cylindrical slice $ABCD$ is dx at rest, and $dx + \psi(x + dx, t) - \psi(x, t)$ at time t . Its mass is that of the slice $A_0B_0C_0D_0$ which is equivalent to $\rho \cdot S \cdot dx$, where S denotes the surface of a section as shown in Figure 2.

The equation of motion of the cylindrical slice $ABCD$ is obtained by applying the fundamental law of dynamics

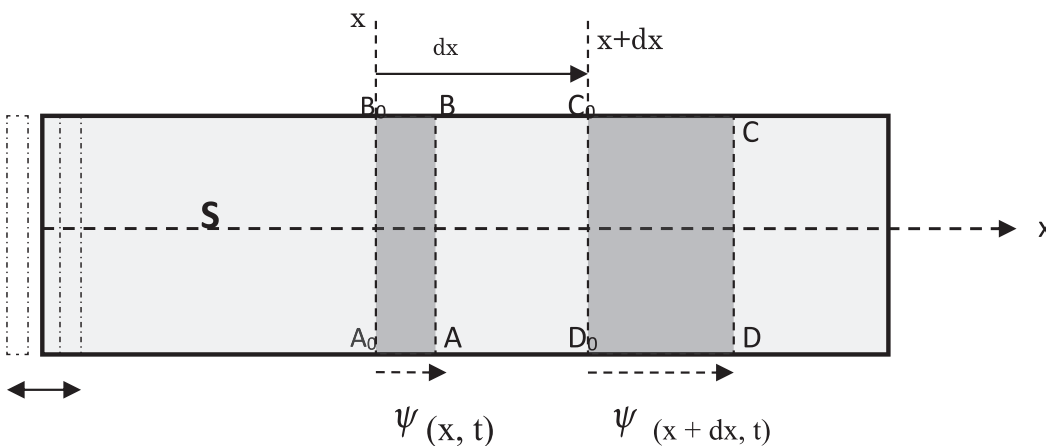


Figure 2. Intake pipe model.

to the cylindrical slice ABCD. The forces to be considered are the occasional F_{oc} and the pressure forces exerted on the AB and CD bases. Hence, the equation of movement is written as:

$$\frac{\partial^2 p^*}{\partial x^2} = \rho K_s \left(\frac{\partial^2 p^*}{\partial t^2} \right) \text{ et } \frac{\partial^2 u^*}{\partial x^2} = \rho K_s \left(\frac{\partial^2 u^*}{\partial t^2} \right) \quad (2)$$

Resolution with the impedance method

The section of the pipe has finite dimensions; one brings back to this section, i.e., to the variation of flow $A^* U^*$ which produces there the acoustic wave, the response of medium at a pressure disturbance p^* . Hence, the concept of characteristic acoustic impedance is represented by Equation 3 as:

$$Z = \frac{p^*}{AU^*} \quad (3)$$

The disturbances created by the acoustic wave being due to the combined effects of two opposite simple waves are therefore written as:

$$\begin{cases} P^* = f_I(c_0 t - x) + f_{II}(c_0 t + x) \\ U^* = \frac{1}{\rho_0 c_0} [f_I(c_0 t - x) - f_{II}(c_0 t + x)] \end{cases} \quad (4)$$

These disturbances are function of the abscissa x of the section where they are observed at time t . The characteristic impedance is then expressed by Equation 5 as:

$$Z(x, t) = \frac{\rho_0 c_0}{A} \frac{f_I(c_0 t - x) + f_{II}(c_0 t + x)}{f_I(c_0 t - x) - f_{II}(c_0 t + x)} \quad (5)$$

In the case of a harmonic acoustic wave, the characteristic impedance of a pipe is independent of time; it is only dependent on the abscissa of the section where, at any time, the acoustic disturbance is observed. Indeed Equation 6 is written as follows:

$$\begin{cases} P^* = B_I e^{j(\omega t - k_0 x)} + B_{II} e^{j(\omega t + k_0 x)} \\ U^* = \frac{1}{\rho_0 c_0} [B_I e^{j(\omega t - k_0 x)} - B_{II} e^{j(\omega t + k_0 x)}] \end{cases} \quad (6)$$

So, the characteristic impedance takes the form of Equation 7 as:

$$Z_x = \frac{\rho_0 c_0}{A} \frac{B_I e^{-jk_0 x} + B_{II} e^{jk_0 x}}{B_I e^{-jk_0 x} - B_{II} e^{jk_0 x}} \quad (7)$$

Optimal intake length

In case of a harmonic acoustic wave, the characteristic impedance of a pipe is time independent; it depends only on the section's abscissa. In this study, the intake pipe is considered as a pipe (with a length equal to "1") closed at the first extremity ($x = 0$) and open at the second ($x = 1$). Thus, the boundary conditions of this tube are:

at abscissa $x=0$ the pipe is open so: $p^*_{(x=0)} = 0 \Rightarrow Z_0 = 0$,
-at abscissa $x=l$ the pipe is closed so: $U^*_{(x=l)} = 0 \Rightarrow Z_l \rightarrow \infty$.

Based on the above conditions, the length of the optimum pipe for having the acoustic supercharging phenomenon is shown in Equation 8 as:

$$f_r = \frac{(2k+1)c_0}{4L} = \frac{c_0}{4\left(\frac{L}{2k+1}\right)} = \frac{c_0}{4L_{2k+1}} \rightarrow \begin{cases} L = \frac{c}{4f_r} \\ L_{2k+1} = \frac{L}{2k+1} \end{cases} \quad (8)$$

where k is the harmonic vibration, that is an integer, f_r is the frequency of propagation of the wave of which it can be determined from the frequency of opening and closing of the valve which is for its part a function of the engine speed (position on the angle of the crankshaft), r denotes the mass stoichiometric ratio, defined as follows: $r = \frac{m_a}{m_c}$

The density of the mixture is expressed by $\frac{1}{\rho_{mél}} = \frac{1+R'}{\rho_c \times R' + \rho_a}$

where R' denotes, the following stoichiometric volume ratio: $R' = \frac{V_c}{V_a}$

The specific heat at constant volume c_v and the specific heat at constant pressure c_p obey the law of mixing. They are determined by the means of elementary heat (c_{vi} , c_{pi}) of the various constituents and the quantities y_i (masses or volumes) of the latter, by the following formulas given in Equation 9:

$$c_{vmél} = \frac{\sum_i x_i \times c_{vi}}{\sum_i x_i} \text{ and } c_{pmél} = \frac{\sum_i x_i \times c_{pi}}{\sum_i x_i} \quad (9)$$

The optimum length can be written in the following forms:

- when operating with gasoline:

$$L = \left(\frac{c_{pe} + \varphi \times r \times c_{pa}}{c_{ve} + \varphi \times r \times c_{va}} \right)^{\frac{1}{2}} \times \left(\frac{RT}{4f_r} \right)^{\frac{1}{2}} \quad (10)$$

- when operating with a gas mixture:

$$L = \left(\frac{c_{pCNG} + c_{pH_2} + \varphi \times \rho_a \times R' \times \left(\frac{y_{CNG}}{\rho_{CNG}} + \frac{y_{H_2}}{\rho_{H_2}} \right) \times c_{pa}}{c_{vCNG} + c_{vCNG} + \varphi \times \rho_a \times R' \times \left(\frac{y_{CNG}}{\rho_{CNG}} + \frac{y_{H_2}}{\rho_{H_2}} \right) \times c_{va}} \right)^{\frac{1}{2}} \times \left(\frac{RT}{4f_r} \right)^{\frac{1}{2}} \quad (11)$$

Equations 10 and 11 allow to calculate the optimum length of the tubing when operating with gasoline and gas mixtures of CNG and hydrogen. This length depends on two variables, the richness, and the frequency.

Air/fuel ratio (AFR) impact on optimal pipe length

Equations 10 and 11 would help to identify the effect of the mixture richness on the mixture length value. While fixing the engine at a well determined speed, the only variable on which the length depends is the richness (φ). Figure 3 shows the variation of the tubing length according to the richness variation. Overall, the richness did not seem to have a significant effect on the length of the pipe when the engine operated on gasoline. However, there was a slight effect on the length of the pipe when the engine operated

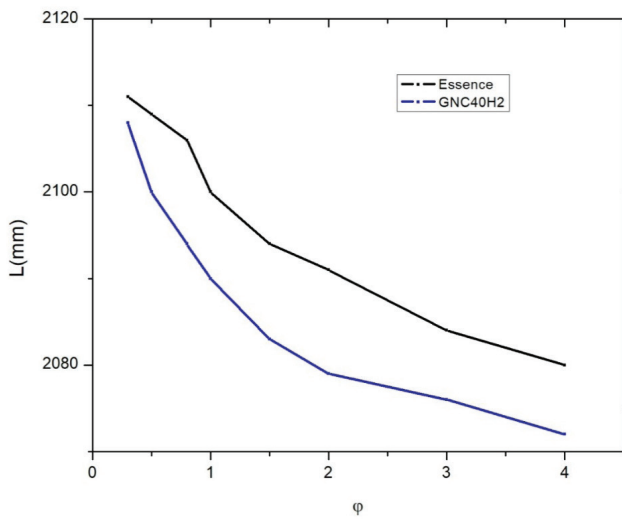


Figure 3. Optimal pipe length variation in function of AFR (gasoline and CNG40H₂)

on CNG. Therefore, it can be induced that operating the engine with hydrogen may deteriorate it. In other words, if the mixture does not respect the stichometry, the engine performance may weaken.

It was observed that the composition of the mixture should be considered in the choice of geometry if the machine makes a broad sweep of richness level during operation. The influence of this richness is clear when the

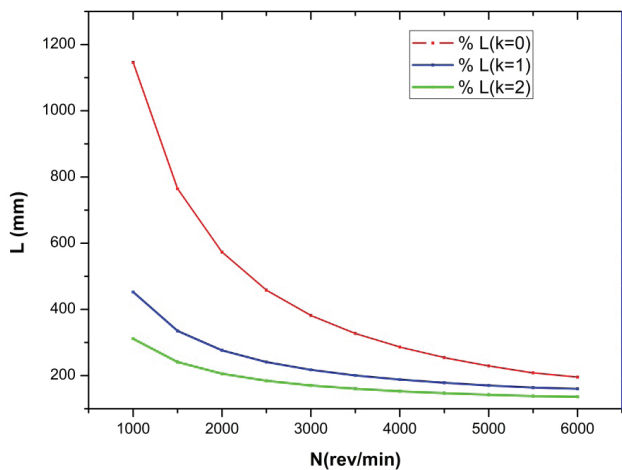


Figure 4. Optimal pipe length variation in function of engine speed (gasoline and CNG40H₂).

engine is running at a speed inferior to 3000 rpm. However, if the mixture was in the turn of a stoichiometric of richness level, its effect would not be significant enough to require change in the pipe’s dimensions and therefore, a fixed geometry would be acceptable according to these criteria.

Engine speed impact on optimal pipe length

As can be seen in Figure 4, the optimum length of the pipe depends on the variation in engine speed. On the other hand, we notice that this dependence ensues from range of engine rotation speed.

For low rotational speeds, it was noted that the nature of the mixture clearly influenced this optimum length. For the idle speed (800 rpm) and the speed which delivers a maximum torque (3500 rpm), it was noted that a difference of 800 mm between the optimal lengths. However, for high engine revolutions, an imperceptible variation is observed.

For speeds ranging between 5000 and 6000 rpm, the differences in pipe length did not show a great effect on engines running on gasoline or on CNG. However, at speeds below 5000 rpm, the differences in geometry seemed to have a big effect. This would imply that a standard length for the two fuels would not be operational. Hence, it would be interesting to design a suitable geometry for every fuel.

EXPERIMENTAL VALIDATION OF THE OPTIMIZED INTAKE MANIFOLD GEOMETRY

Adjustment of the Pipe Length

Firstly, it should be noted that only one pipe length, 3000 rpm, was adopted for the experimental work because it was considered the most common rotation frequency for

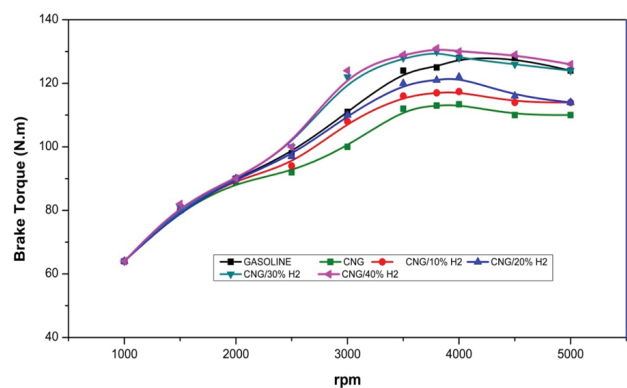


Figure 5. Brake torque (BT) in function of engine speed.

Table 3. Optimal intake pipe length

Harmonic k	0	1	2	3
Gasoline	2100	423	299	213
CNG-40H2	2090	418	298	213

engines. Secondly, it was observed that the rotation frequency between the couples delivering the mixtures was inconsistent with this engine. Therefore, it was deemed very important to determine the geometry that would be most adequate to benefit from natural supercharging to input some economic and mechanical benefits.

As can be noticed in Figure 5, different fuels yielded different torque values starting from a frequency of 2000 rpm to a frequency of 4500 rpm. However, the frequency that yielded the maximum torque was 3600 rpm of an engine operating on CNG/40%H₂. Therefore, Table 3 exhibits the optimum pipe lengths required for a unit richness level.

Addition of a Cooling Pipe

Because of the hydrogen low self-ignition property, and to cushion the anomalies relating to hydrogen friction with

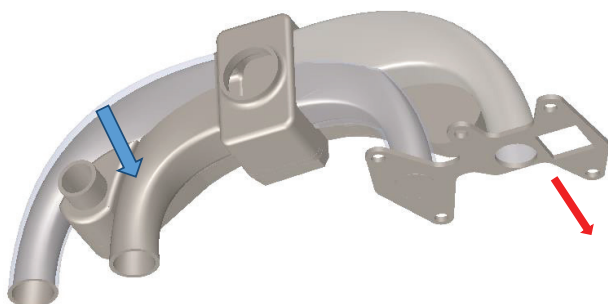


Figure 6. The manifold with different pipes lengths and a cooling intake.

hot walls, a second solution was proposed. The new geometry was provided with a cooling system, as shown in Figure 6.

Effect of the Optimized Intake Geometry on Engine Behavior

Figure 7 displays the test bench with the new cooled manifold. The manifold was assembled to the engine. The collector was cooled by the engine cooling water. The coolant inlet port of the manifold was directly attached to the radiator outlet line after circulating through the collector water was discharged at the pump’s inlet for a better cooling.

After the assembling stage, a series of tests were conducted to characterize the performance and emissions of the new manifold-equipped engine. For this purpose, the measurement of the volumetric efficiency of the engine was tested through the measurement of the air/fuel charge in the cylinder. This was achieved by measuring the maximum pressure in the cylinder when the piston was at the top dead center (TDC). These measurements were compared with those recorded for the manifold old geometry. Figure 8 displays histograms of the maximum in-cylinder pressure at TDC for old and new geometries at different engine rates.

Firstly, as can be clearly observed, the pressure recorded at all the engine rates was higher for the engine with new geometry (NG) than the one recorded with the old geometry (OG). Secondly, this difference is slight for the regimes far from those chosen for the pipes’ dimensioning, which is a consequence of the pipes which have become shorter. The shorter pipes are, the less friction and pressure drop will occur, which justifies the increase in pressure for the new geometry. It is worth noting that the pressure difference is



1- Engine; 2- New intake manifold; 3-mixer Air/CNG-H₂.

Figure 7. Test bench with the new cooled manifold.

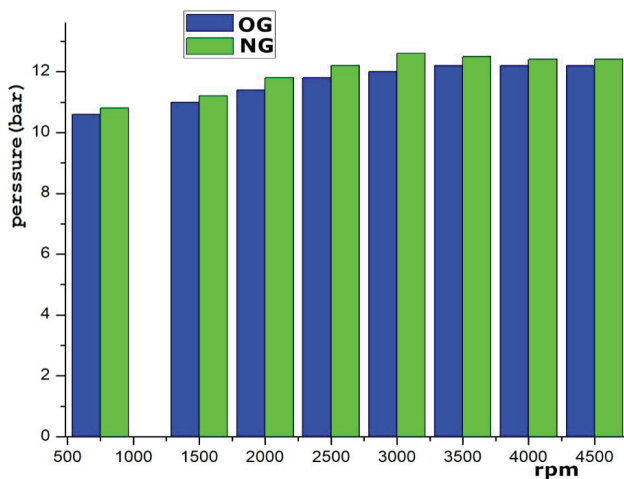


Figure 8. Maximum in-cylinder pressure at TDC.

maximum for the design regime, which justifies the contribution generated by natural overeating.

Impact of the New Geometry on the Optimum Hydrogen Ratio Addition

The second finding was related to the optimum amount of H₂ that could be added to CNG without adversely affecting the normal engine operation or leading to degradation of performance. Figure 9 illustrates the in-cylinder pressure in function of CA°. The fuels used in this experiment were CNG-50H or gasoline. Figure 9 also exhibits a comparison between the pressure of cylinders of engines equipped with the old and new geometry of the manifold. Figures 10 clearly shows that at 3500 rpm, the addition of 50% H₂ to the CNG allowed the engine to run smoothly with the new optimized manifold geometry.

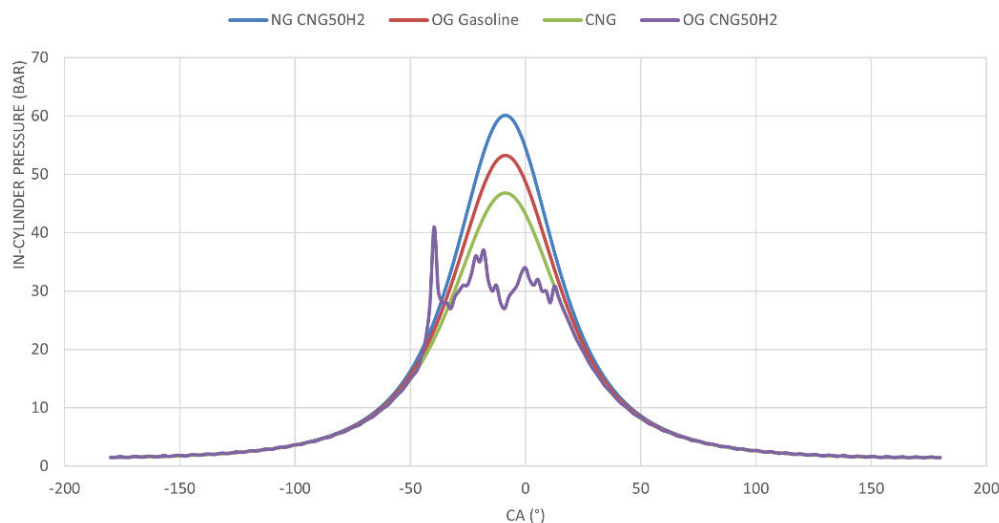


Figure 9. In-cylinder pressure as function of CA°.

These results revealed that the addition of 50% of H₂ with the new geometry had rather beneficial effects on the engine performance since the maximum value of the pressure was obtained for the CNG-50H₂. Indeed, as can be seen in Figure 9, the highest in-cylinder pressure, 60 bar, was obtained with NG CNG-50H₂. This finding differs from the work of Saaidia et al. [28] who reported that the optimum fraction of hydrogen with CNG was 40% for an anomaly-free operation. Also, it was observed that the equal proportion of CNG and H₂ allowed the engine to run normally without the occurrence of the back-fire anomaly. In addition, two more conditions were required for the optimum operation of the engine. The first was related to the fact that the evolution of the pressure in the cylinder during the intake. Compression and expansion phases were conceived as a function of the crankshaft angle. Moreover, the engine speed was set at 3200 rpm. This rotation frequency was chosen because the engine produced its maximum BT at this speed when it was supplied with a mixture of CNG-H₂ as indicated above. Finally, the pressure control allowed us to monitor the presence or absence of pre-ignition or abnormal combustion. In addition, it is revealed that the addition of 50% of H₂ with the new geometry has a rather beneficial effect on the performance since the maximum value of the pressure is obtained for the fuel containing a fraction of 50% with the CNG.

Effects of the Optimized Intake Manifold on Engine Emissions

This part deals with the engine behavior in terms of emissions while comparing the old geometry with the new one. Series of tests are carried out with a mixture containing 40% of H₂ with CNG (GNC/40H₂). Emissions levels of NO_x, HC and CO are shown in Figures 10, 11 and 12. All

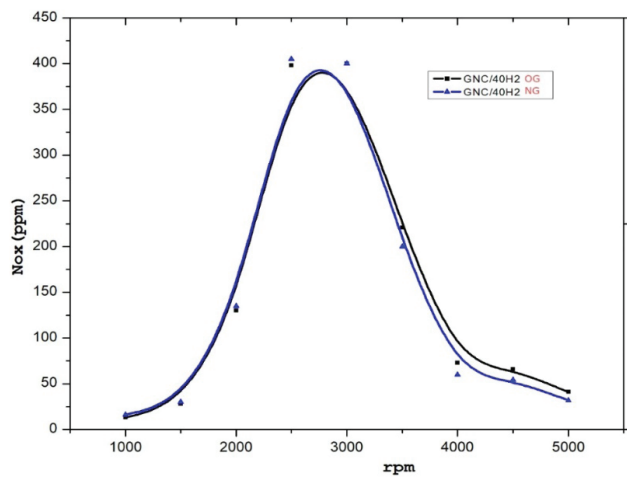


Figure 10. NOx concentration as function of engine speed.

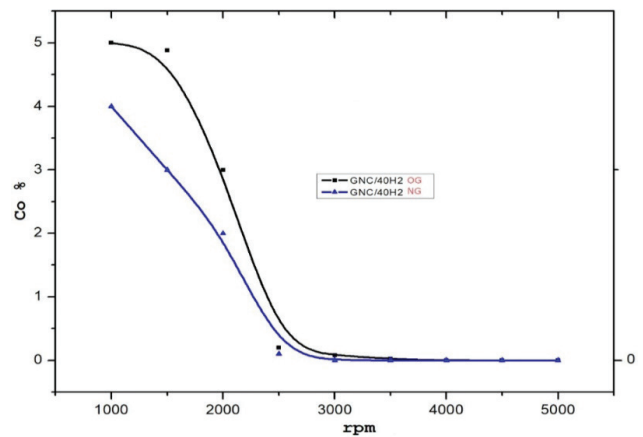


Figure 11. CO concentration in OG and NG engines as function of engine speed.

the tests were conducted with OG and NG engine operating on CNG-40H2 at different speeds.

The first observation was that NOx emission practically identical to both geometries at speeds inferior or equal to 3200 rpm. This quasi equality of NOx emission can be explained by the fact that combustion at lower temperatures of the engine is not complete, and this condition is particularly favorable for NOx formation. However, at speeds above 3200 rpm the new intake manifold would provide excellent ventilation of the cylinders, which would improve the combustion and help to emit fewer NOx particles.

Figure 11 shows CO concentration in OG and NG engines in function of engine speed. From the figure it is

clearly clear that CO concentration seemed to depend on the engine speed. For both engines, with OG and NG, CO was much higher at lower rotation rates ranging between 1000 rpm and 2500 rpm. At higher rotation rates, >2500, CO concentrations tended to stabilize at 0%. However, it can be clearly observed that CO concentration in the NG engine was much lower than the one in the OG engine. Indeed, whereas CO concentration was 5% at 1000 rpm in the OG engine, this value was only 4% in the NG engine. The CO concentrations in the OG engine continued to be higher than that in the NG engine until both engines reached 3500 rpm. At this point both CO concentrations stabilized at 0%. The decrease and final stabilization of CO

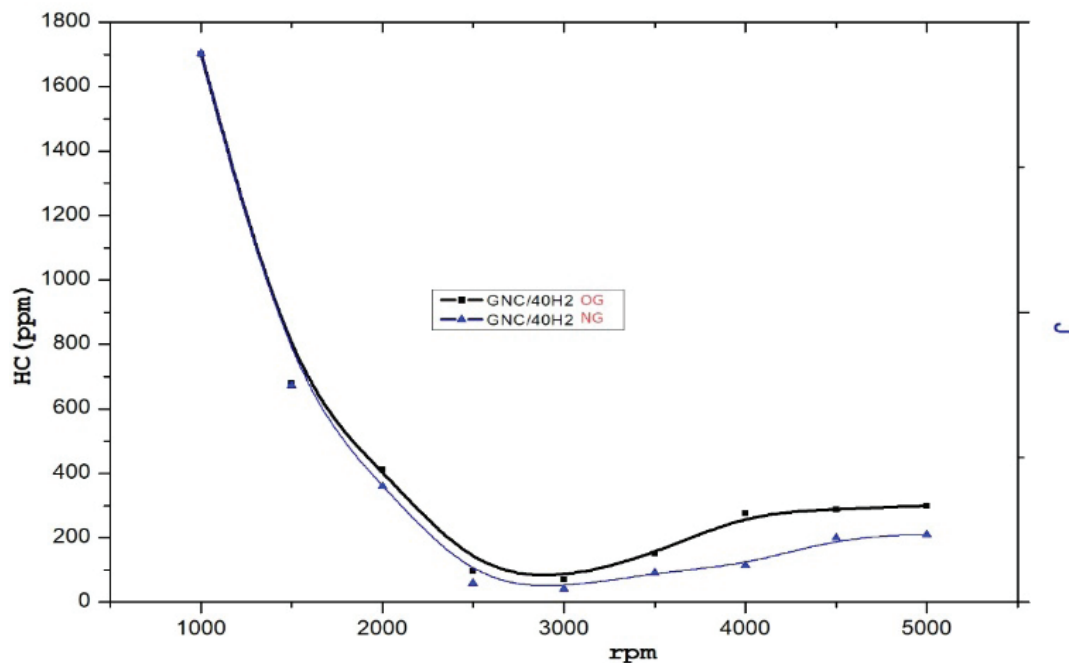


Figure 12. HC concentration as function of engine speed.

concentration can be explained by the fact that hydrogen combustion would be complete at high speeds due to the physical properties of hydrogen and its flame propagation speed.

Figure 12 shows HC concentration in function of engine speed. Firstly, the existence of CH gas could be linked to the insufficient air in the combustion chambers. Secondly, as can be seen in figure 12, at speeds between 1000 and 1500 rpm, the concentration of HC particles reached 1700 ppm for both OG and the NG engine collectors. This can be explained by the fact that low speeds of admission would generate a considerable decrease in the pressure. This finding would confirm the observation reported in figure 11 above, where hydrogen was reported to show an incomplete combustion at low speeds. Thirdly, figure 12 shows that the faster the engine runs, the lower CH emission is. At 3000 rpm, both geometries reached the lowest CH emissions. However, the engine with the NG collector presented a slightly lower CH emission than the engine with the OG collector. This can be explained by the better filling provided by the NG collector. Finally, despite the slight increase of CH emission above 3000 RPM, the engine with the NG collector stabilized at a CH emission of 2000 ppm, while that with the OG collector stabilized at 3000 rpm.

CONCLUSION

This study used the analytical acoustic method to predict the optimal intake pipes lengths for engines running on a mixture of hydrogen and CNG. The geometry of the intake manifold plays a crucial role in determining the in-cylinder flow characteristics of an internal combustion engine. The intake manifold is responsible for delivering the air-fuel mixture to the combustion chambers, and its design can significantly impact engine performance. The shape and length of the intake manifold runners influence the distribution of airflow to individual cylinders. If the lengths or diameters of the runners are not properly matched, there may be variations in the amount of air reaching each cylinder. This can result in an imbalance in the combustion process, leading to reduced engine efficiency and power output. The shape and size of the intake manifold runners affect the air velocity entering the combustion chamber. Higher air velocity promotes better air-fuel mixing, which is essential for efficient combustion. A well-designed intake manifold ensures a smooth and controlled flow of air, optimizing the air-fuel mixture preparation.

The main findings showed that the optimized manifold presented an advantage of natural supercharging. This study confirmed the choice of the length of the intake manifold pipes. Moreover, to ensure a better filling, the optimized manifold proved to reduce both the amount of residual fuel in the pipes and the problems of backfire and auto-ignition when hydrogen is used. Furthermore, NG manifold wide the range of the fraction of hydrogen admissible up to a content of 50% hydrogen of CNG for normal

engine operation. Finally, with the introduction of a cooling system for the intake manifold, this study revealed that the performance and safety of the engine reduced the danger of overheating from friction between hydrogen and the engine walls. Finally, the optimized NG collector showed fewer polluting emissions because of its improved combustion. These findings may have very beneficial implications for industry, economy, and environment.

NOMENCLATURE

ICE	Internal combustion engines
f	Frequency of rotation (Hz)
f_r	Resonance frequency (Hz)
k	Vibration harmonic
K_t	Isothermal compressibility coefficient
K_s	Isentropic compressibility coefficient
M_{mel}	Mixture mass (kg)
P^*	Relative over-pressure (Pa)
r	Mass stoichiometric ratio
t_f	Engine vibration period (s)
Z	Specific acoustic impedance (Pa.s.m ⁻¹)
ψ	Displacement of a gas slice (mm)
φ	Air fuel ratio
CNG	Compressed natural gas.
H ₂ CNG	Compressed natural gas and hydrogen mixture

AUTHORSHIP CONTRIBUTIONS

Authors equally contributed to this work.

DATA AVAILABILITY STATEMENT

The authors confirm that the data that supports the findings of this study are available within the article. Raw data that support the finding of this study are available from the corresponding author, upon reasonable request.

CONFLICT OF INTEREST

The author declared no potential conflicts of interest with respect to the research, authorship, and/or publication of this article.

ETHICS

There are no ethical issues with the publication of this manuscript.

REFERENCES

- [1] Heywood JB. Internal combustion engines fundamentals. New York: McGraw Hill; 1988.
- [2] Sharma VK, Mohan M, Mouli C. Effect of intake swirl on the performance of single cylinder direct injection diesel engine. IOP Conf Ser Mater Sci Eng 2017;263:062077. [[CrossRef](#)]

- [3] Priyadarsini I. Flow analysis of intake manifold using computational fluid dynamics. *Int J Eng Adv Res Technol* 2016;2:1–5.
- [4] Chaubey A, Tiwari AC. Design and CFD analysis of the intake manifold for the Suzuki G13bb engine. *Int J Res Appl Sci Eng Technol* 2017;5:1258–1276.
- [5] Battista D, Bartolomeo M, Cipollone R. Flow and thermal management of engine intake air for fuel and emissions saving. *Energy Convers Manag* 2018;173:46–55. [\[CrossRef\]](#)
- [6] Silva E, Ochoa A, Henriquez J. Analysis and runners length optimization of the intake manifold of a 4-cylinder spark ignition engine. *Energy Convers Manag* 2019;188:310–320. [\[CrossRef\]](#)
- [7] Giannakopoulos GK, Frouzakis CE, Boulouchos K, Fischer PF, Tomboulides AG. Direct numerical simulation of the flow in the intake pipe of an internal combustion engine. *Int J Heat Fluid Flow* 2017;68:257–268. [\[CrossRef\]](#)
- [8] Benajes J, Reyes E, Galindo J, Peidro J. Predesign Model for Intake Manifolds in Internal Combustion Engines. Society of Automotive Engineers, Inc., Paper SAE 1997:970055. [\[CrossRef\]](#)
- [9] Chalet D, Mahe A, Migaud J, Hetet JF. A frequency modeling of the pressure waves in the inlet manifold of internal combustion engine. *Appl Energy* 2011;88:2988–2994. [\[CrossRef\]](#)
- [10] Chalet D, Chesse P. Analysis of unsteady flow through a throttle valve using CFD. *Eng Appl Comput Fluid Mech* 2010;4:387–395. [\[CrossRef\]](#)
- [11] Costa RC, Hanriot SM, Sodr e JR. Influence of intake pipe length and diameter on the performance of a spark ignition engine. *J Braz Soc Mech Sci Eng* 2014;36:29–35. [\[CrossRef\]](#)
- [12] Sadeq AM, Bassiony MA, Elbashir AM, Ahmed SF, Khraisheh M. Combustion and emissions of a diesel engine utilizing novel intake manifold designs and running on alternative fuels. *Fuel* 2019;255:115769. [\[CrossRef\]](#)
- [13] Sadeq AM, Bassiony MA, Elbashir AM, Ahmed SF, Khraisheh M. Combustion and emissions of a diesel engine utilizing novel intake manifold designs and running on alternative fuels. *Fuel* 2019;255:115769. [\[CrossRef\]](#)
- [14] Hennings S, Moura LM, Mariani VC, Coelho S, Vel squez JA. Volumetric efficiency optimization of a single-cylinder D.I. diesel engine using differential evolution algorithm. *Appl Therm Eng* 2016;108:660–669. [\[CrossRef\]](#)
- [15] Vaz J, Machado A, Martinuzzi R, Martins M. Design and Manufacture of a Formula SAE Variable Intake Manifold. SAE Technical Paper 2017;36:0181. [\[CrossRef\]](#)
- [16] Gocmen K, Soyhan HS. An intake manifold geometry for enhancement of pressure drop in a diesel engine. *Fuel* 2020;261:116193. [\[CrossRef\]](#)
- [17] Harrison MF, Soto I, Unzueta P. A linear acoustic model for multicylinder IC engine intake manifolds including the effects of the intake throttle. *J Sound Vib* 2004;278:975–1011. [\[CrossRef\]](#)
- [18] Hadjkacem S, Jemni MA, Abid MS. Volumetric efficiency optimization of manifold with variable geometry using acoustic vibration for intake manifold with variable geometry in case of lpg-enriched hydrogen engine. *Arab J Sci Eng* 2019;44:731–738. [\[CrossRef\]](#)
- [19] Hiereth H, Prenninger P. *Charging the Internal Combustion Engine*. New York, Wien: Springer; 2007.
- [20] Borel M. *Les ph nom nes d'ondes dans les moteurs*. Publications de l'Institut Fran ais du P trole,  ditions Technip: France; 2000.
- [21] Desmond EW, Richard JP. *Theory of Engine Manifold Design: Wave Action Methods for IC ENGINES*. London: Professional Engineering Pub; 2000.
- [22] Jemni MA, Kantchev G, Abid MS. Influence of intake manifold design on in-cylinder flow and engine performances in a bus diesel engine converted to LPG gas fueled, using CFD analyses and experimental investigations. *Energy* 2011;36:2701–2715. [\[CrossRef\]](#)
- [23] Samuel J, Annamalai K. Effect of variable length intake manifold on a turbocharged multi-cylinder diesel engine. SAE Technical Paper 2013:01-2756. [\[CrossRef\]](#)
- [24] Bortoluzzi D, Cossalter V, Doria A. The effect of tunable resonators on the volumetric efficiency of an engine. SAE Technical Paper 1998:983045. [\[CrossRef\]](#)
- [25] Margary R, Nino E, Vafidis C. The effect of intake duct length on the in-cylinder air motion in a motored diesel engine. SAE Technical Paper 1990:900057. [\[CrossRef\]](#)
- [26] Maftouni N, Ebrahimi R. The effect of intake manifold runners' length on the volumetric efficiency by 3-D CFD model. SAE Technical Paper 2006:2006-32-0118. [\[CrossRef\]](#)
- [27] Fontana G, Bozza F, Galloni E, Siano D. Experimental and numerical analyses for the characterization of the cyclic dispersion and knock occurrence in a small-size SI engine. SAE Technical Paper 2010:2010-32-0069. [\[CrossRef\]](#)
- [28] Saaidia R, Jemni MA, Abid MS. Simulation and empirical studies of the commercial SI engine performance and its emission levels when running on a CNG and hydrogen blend. *Energies* 2018;11:29. [\[CrossRef\]](#)
- [29] Aezeden M, Kuri P, Rout S, Muduli K. Assessment of ec-toxicity potential of fuel by exhaust gas analysis. *J Therm Eng* 2023;9:669–678. [\[CrossRef\]](#)
- [30] Attia ME. CFD Simulation of the Co Emissions of Pollutants Contained in Flames H2-C3H8/Air. 2020 International Conference on Renewable Energy Integration into Smart Grids: A Multidisciplinary Approach to Technology Modelling and Simulation (ICREISG), Bhubaneswar, India, 2020:222–227.